DOI: 10.1534/genetics.105.048736

l7Rn6 Encodes a Novel Protein Required for Clara Cell Function in Mouse Lung Development

Rodrigo Fernández-Valdivia,*,[1] Ying Zhang,* Sonia Pai,* Michael L. Metzker*,† and Armin Schumacher*,[2]

**Department of Molecular and Human Genetics and †Human Genome Sequencing Center, Baylor College of Medicine, Houston, Texas 77030*

Manuscript received July 24, 2005
Accepted for publication September 6, 2005

ABSTRACT

The highly secretory Clara cells play a pivotal role in protecting the lung against inflammation and oxidative stress. This study reports the positional cloning of a novel protein required for Clara cell physiology in mouse lung development. The perinatal lethal *N*-ethyl-*N*-nitrosourea-induced *l7Rn6*^{4234SB} allele contained a nonsense mutation in the previously hypothetical gene NM_026304 on chromosome 7. Whereas *l7Rn6* mRNA levels were indistinguishable from wild type, *l7Rn6*^{4234SB} homozygotes exhibited decreased expression of the truncated protein, suggesting protein instability. During late gestation, l7Rn6 was widely expressed in the cytoplasm of lung epithelial cells, whereas perinatal expression was restricted to the bronchiolar epithelium. Homozygosity for the *l7Rn6*^{4234SB} allele did not affect early steps in lung patterning, growth, or cellular differentiation. Rather, mutant lungs demonstrated severe emphysematous enlargement of the distal respiratory sacs at birth. Clara cell pathophysiology was evident from decreased cytoplasmic CCSP and SP-B protein levels, enlargement and disorganization of the Golgi complex, and formation of aberrant vesicular structures. Additional support for a role in the secretory pathway derived from l7Rn6 localization to the endoplasmic reticulum. Thus, l7Rn6 represents a novel protein required for organization and/or function of the secretory apparatus in Clara cells in mouse lung.

THE highly secretory Clara cells represent nonciliated columnar cells, which, along with ciliated cells, line the bronchiolar epithelium (Ten Have-Opbroek 1991). Clara cell functions include cell renewal of airway epithelium following injury, for example, from ozone exposure (Evans *et al.* 1976, 1978). Furthermore, these cells express CCSP (also known as uteroglobin or blastokinin), a 16-kDa homodimeric protein, which protects the respiratory tract against oxidative stress, inhibits phospholipase A2, and exhibits antiinflammatory and immunomodulatory activities (Johnston *et al.* 1997; Mango *et al.* 1998; Broeckaert *et al.* 2000; Singh and Katyal 2000; Chen *et al.* 2001; Watson *et al.* 2001). Other proteins produced and presumably secreted by Clara cells include phospolipase A, surfactant proteins A, B, and D (SP-A, SP-B, and SP-D) (Phelps and Floros 1991; Kalina *et al.* 1992; Singh and Katyal 2000), CC26, a 26-kDa selenium-independent glutathione peroxidase (Power and Nicholas 1999), as well as several members of the cell surface integrin family (Blundell and Harrison 2005).

Recent studies in humans and mice have linked abnormal levels of secretory proteins with defects in lung homeostasis. In humans, surfactant deficiency resulted in respiratory distress syndrome, the most frequent cause of lethality and morbidity in infants of <1 year of age (Nogee *et al.* 1994; Cole *et al.* 2001; Shulenin *et al.* 2004). Likewise, targeted ablation of the gene encoding SP-B resulted in respiratory failure in newborn mice and death shortly after birth (Clark *et al.* 1995). Conditional deletion of winged helix transcription factor Foxa2 caused a significant reduction in the expression of CCSP, SP-A, SP-C, and SP-B as well as emphysematous enlargement of the lungs, decreased alveolar septation, goblet cell hyperplasia, and increased neutrophil infiltration (Wan *et al.* 2004a,b). Interestingly, premature human newborns with bronchopulmonary dysplasia demonstrated increased CCSP oxidation and decreased CCSP protein levels in tracheal aspirate, supporting an important role of Clara cells in lung homeostasis at birth (Ramsay *et al.* 2001).

Here we report the positional cloning of the *N*-ethyl-*N*-nitrosourea (ENU)-induced *l7Rn6*^{4234SB} mutation and identify the previously hypothetical gene NM_026304 as the *l7Rn6* locus. Phenotypic and marker gene expression analysis revealed a pivotal role for l7Rn6 in Clara cell function in mouse lung development. In addition to a perinatal emphysematous lung phenotype, *l7Rn6*^{4234SB} Clara cells demonstrated decreased cytoplasmic CCSP

[1]*Present address:* Department of Molecular and Cell Biology, Baylor College of Medicine, Houston, TX 77030.

[2]*Corresponding author:* Department of Molecular and Human Genetics, Baylor College of Medicine, One Baylor Plaza, S-803, Houston, TX 77030. E-mail: armins@bcm.tmc.edu

and SP-B protein levels, significant enlargement and disorganization of the Golgi complex, as well as aberrant vesicular structures. Since early patterning, growth, or cellular differentiation appeared unaffected, we suggest that secretory defects in Clara cells might govern the perinatal emphysematous phenotype in *l7Rn6*^{4234SB} homozygous lungs.

MATERIALS AND METHODS

Animals and genotyping: The *l7Rn6*^{4234SB} allele used in this study was isolated in an ENU mutagenesis screen to recover (pseudo-)recessive mutations in the *albino* (*c*) region (Rinchik *et al.* 1990). The *l7Rn6*^{4234SB} allele is closely linked to *c* on distal chromosome 7 and was maintained on a mixed genetic background opposite a wild-type chromosome marked by the *chinchilla* (c^{ch}) locus, a partial loss-of-function allele at the *tyrosinase* locus (Rinchik and Carpenter 1993, 1999). Following identification of the *l7Rn6*^{4234SB} point mutation in NM_026304, primers 5′-TACAAATTTGGATTTTCTTTTCTA GTTA (forward) and 5′-GGTAGGTTTCATGACCCTTTTGAC (reverse) were used for direct genotyping. The forward primer contains a thymine instead of a guanine in the -3 position compared with wild-type sequence, which, in the context of the *l7Rn6*^{4234SB} T → A transversion, creates a diagnostic *Mse*I restriction enzyme site for the mutant allele.

The transgenic rescue construct encompassed an ~6.3-kb *Eco*RI fragment with the putative *l7Rn6* promoter, which was cloned upstream of a KCR cassette containing intronic sequences from the rabbit β-*globin* locus to augment transgene expression (Ma *et al.* 1999). In addition, a heterologous 3′-UTR containing the bovine growth hormone polyadenylation signal (Tepera *et al.* 2003) was cloned downstream of the full-length *l7Rn6* (NM_0263040) open reading frame (Figure 1, A and D). Two founder lines (*A1tg* and *A4tg*) were obtained from injection of the linearized construct into the pronuclei of FVB/NJ zygotes. The line with the higher expression level *A4tg* was crossed with *l7Rn6*$^{4234SB/+}$ animals for rescue experiments. Following one backcross onto the FVB/NJ background, *l7Rn6*$^{4234SB/+}$; *A4tg* animals were intercrossed to assess transgenic rescue on an ~75% FVB/NJ background. The presence of the transgene was detected by PCR using primers 5′-GAAC TTCAGGCTCCTGGGCAAC (forward) and 5′-ACCAGGCAG CCAAACATG (reverse). The Institutional Animal Care and Use Committee of Baylor College of Medicine approved all animal experiments in this study.

Genomic mapping of candidate genes: Candidate genes were mapped to the *l7Rn6* critical region by PCR amplification of the first and last exon of each candidate gene from several yeast artificial chromosomes (YACs) spanning the 150-kb candidate region (Holdener *et al.* 1995). The following primers were used: 5′-TTAGGAAGGAAGGGTCAGAGGTCG (forward) and 5′-ACCAGGCAGCCAAACATG (reverse) for the first exon of *l7Rn6* (NM_026304), 5′-CACAGAACCCCCTCTTTTGG (forward) and 5′-GCCTCCAAGAAGTATGTCACAC (reverse) for the last exon of *l7Rn6* (NM_026304), 5′-CTTCTTAGTTCAG CAACCCTCC (forward) and 5′-GCACTAAGGTGACTTTCCCAC (reverse) for the first exon of AK014876, and 5′-GCTGTTTCT CTTGGATCAGTG (forward) and 5′-CTCGGGAAATAGTAGG TTCAAGCG (reverse) for the last exon of AK014876.

cDNA cloning and mRNA expression analysis: Total RNA was isolated using TRIzol Reagent (Invitrogen, Carlsbad, CA). Five micrograms of total RNA were reverse transcribed using oligo (dT) priming and M-MLV reverse transcriptase (Invitrogen) as described (Mok *et al.* 2004a). Primers used for cDNA cloning included: 5′-TTAGGAAGGAAGGGTCAGAGG TCG (forward) and 5′-GCCTCCAAGAAGTATGTCACAC (reverse) for *l7Rn6* (NM_026304), as well as 5′-GTGGGAAAGT CACCTTAGTGC (forward) and 5′-CTCGGGAAATAGTAG GTTCAAGCG (reverse) for AK014876. Expression levels of the transgenic lines *A1tg* and *A4tg* and endogenous *l7Rn6* (NM_026304) were analyzed by semiquantitative RT-PCR from brain, lung, heart, liver, kidney, and muscle. The following primers were used: 5′-GTTGGACAGTCTGGCTCAGCAG (forward) and 5′-GGTAGGTTTCATGACCCTTTTGAC (reverse) for *l7Rn6* (NM_026304), 5′-AGCCATGTACGTAGCCATCC (forward) and 5′-TTTGATGTCACGCACGATTT (reverse) for β-*actin*, and 5′-TGCGGAATTCCTGCAGCC (forward) and 5′-CACCCCATTTGAATCAGGATAGGA (reverse) for the transgene.

Histology: Lungs were dissected between embryonic day 15.5 (E15.5) and postnatal day 0 (P0) and fixed overnight in 4% paraformaldehyde. P0 lungs were inflated with paraformaldehyde; lung weight was ascertained before inflation. Following fixation, lungs were dehydrated in a graded series of ethanol, embedded in paraffin, and sectioned at 5 μm. Airway dilation was quantified by determination of mean linear intercepts as described previously (Dunnill 1962). Briefly, six horizontal lines were drawn onto digital images, taken at ×200 magnification, from randomly selected, hematoxylin-eosin (H&E)-stained P0 lung sections. The number of times each line crossed a saccular wall was counted. Results are expressed as the total number of intercepts divided by the total length of the six lines. Five independent lung sections per animal, and at least six animals per genotype were analyzed. All data are reported as the means ± SD. Statistical analysis was performed using Student's unpaired *t*-test. P0 lungs from *l7Rn6*$^{4234SB/4234SB}$ and wild-type littermates were analyzed by electron microscopy. Dissected lungs were inflated with phosphate-buffered 2.5% glutaraldehyde solution and fixed for 12 hr at 4°. Samples were processed and analyzed as described previously (Ray *et al.* 1996).

Immunohistochemistry and mRNA *in situ* hybridization: A polyclonal αl7Rn6 antiserum was raised in rabbits against amino acids 20-34 (EDKFVFDLPDYENINH) and purified by immunoaffinity. Antibodies were used at the following dilutions: αl7Rn6 at 1:400, αSP-A (Chemicon) at 1:200, αSP-B (Chemicon) at 1:200, αSP-C (Chemicon) at 1:250, αCCSP (Santa Cruz Biotechnology) at 1:100, αCGRP (Santa Cruz Biotechnology) at 1:200, and αCC26 (Chemicon) at 1:500. E15.5 embryos as well as dissected E16.5-P0 lungs were processed for immunohistochemistry as described previously (Mok *et al.* 2004b). Sections were incubated with biotinylated secondary antibodies and horseradish peroxidase-conjugated streptavidin using the Vectastain Elite ABC Kit (Vector Laboratories, Burlingame, CA). Vector NovaRED substrate (Vector Laboratories) was used for signal detection. Sections from both *l7Rn6*$^{+/+}$ and *l7Rn6*$^{4234SB/4234SB}$ lungs were mounted side by side on the same slide to allow for comparison of staining intensity.

For mRNA *in situ* hybridization on lung sections, digoxigenin-11-UTP-labeled antisense cRNA probes were prepared as described (Wilkinson and Nieto 1993). A 0.5-kb *ccsp* mRNA *in situ* hybridization probe was kindly provided by F. DeMayo. Sense *ccsp* cRNA probe served as a negative control. mRNA *in situ* hybridization to sectioned lungs was performed as described previously with minor modifications (Neubüser *et al.* 1995). Briefly, 5-μm parasagittal sections were hybridized overnight at 65° with digoxigenin-11-UTP-labeled antisense cRNA probes in a buffer containing 50% deionized formamide, 5× SSC, 50 μg/ml heparin, 0.1% Tween-20, 100 μg/ml tRNA, 5% dextran sulfate, and 8 mm citric acid. Following hybridization, sections were washed and incubated with an anti-digoxygenin antibody (Roche). To ensure comparability, the antisense and sense probe experiments were conducted

under the same conditions, including the duration of the alkaline phosphatase detection reaction.

Western blot analysis: Lungs were homogenized in lysis buffer containing 20 mM Tris, pH 7.5, 150 mM NaCl, 1 mM EDTA, 1 mM EGTA, 1% Trixton X-100, and EDTA-free protease inhibitor (Complete, Roche). Protein lysates were quantified using BIORAD DC Protein Assay kit (Bio-Rad). The samples were mixed with equal volume of 2× sample buffer containing β-mercaptoethanol and boiled for 5 min. Twenty-five micrograms of protein were loaded per lane and separated on 10 or 15% SDS-PAGE, followed by transfer to PVDF membrane (Bio-Rad). Membranes were blocked by incubation in 5% BSA in TBS containing 0.1% Tween 20 for 2 hr at room temperature (RT), and then incubated with primary antibodies for 12 hr at 4°. Antibodies were used at the following dilutions: αl7Rn6 at 1:4000, αMAC3 (BD Biosciences) at 1:2000, and anti-β-Actin (Santa Cruz Biotechnology) at 1:2000. Membranes were incubated with horseradish peroxidase-conjugated secondary antibodies at 1:5000, and signals were developed using Enhanced Chemiluminescence System (Santa Cruz Biotechnology).

Indirect immunofluorescence microscopy: A549 lung carcinoma cells were grown overnight at 37° on slides coated with poly(D)-lysine (BD Biosciences) and collagen (Sigma, St. Louis). Slides were fixed in 100% prechilled methanol for 5 min at −20° and rehydrated in PBS for 10 min at RT. Following blocking with 5% donkey or goat serum for 30 min at RT, cells were incubated overnight with sets of primary antibodies: αl7Rn6 (NM_026304) (1:50 dilution)/αCCSP (Santa Cruz; 1:50), αl7Rn6 (NM_026304) (1:50)/αCalnexin (Chemicon; 1:500), αl7Rn6 (1:50)/αGS28 (BD Biosciences; 1:50), and αl7Rn6 (NM_026304) (1:50)/anti-α-SNAP (Stressgen; 1:50). The cells were washed three times with PBS and incubated with fluorophore-conjugated secondary antibodies at 1:250 dilution for 1 hr at RT. The secondary antibodies included Cy3-conjugated donkey anti-goat-IgG, Cy3-conjugated goat-anti-mouse IgG, Alexa 488-conjugated goat-anti-rabbit IgG (all from Jackson ImmunoResearch), and Alexa 488-conjugated donkey-anti-rabbit IgG (Molecular Probes, Eugene, OR). Slides were mounted with Vectashield mounting medium (Vector). Confocal microscopy was performed on an LSM 510 laser scanning microscope system (Zeiss, Thornwood, NY) equipped with argon and HeNe laser at an excitation of 488 and 543 nm, respectively. Slides were viewed with ×63 microscope objectives. Images were collected and processed with LSM 5 system software (Zeiss) and edited with Image J, AxioVisionAC, and Adobe Photoshop software packages.

RESULTS

Perinatal lethality in *l7Rn6*^{4234SB} homozygotes: Homozygosity for the *l7Rn6*^{4234SB} allele was largely compatible with embryonic development and ~80% of the mutants survived to birth (data not shown). However, the vast majority of *l7Rn6*^{4234SB} homozygotes died within 24 hr after birth and all pups were dead within 48 hr. Mutant pups frequently demonstrated cyanosis shortly before death. Histological analysis did not reveal any gross abnormalities or patterning defects in vital organs and tissues, such as brain, heart, liver, kidney, and skeletal muscle (data not shown). Furthermore, metabolic screening for abnormal urine organic acids and serum amino acids did not detect any significant differences between *l7Rn6*$^{4234SB/4234SB}$ and wild-type pups at birth (data not shown).

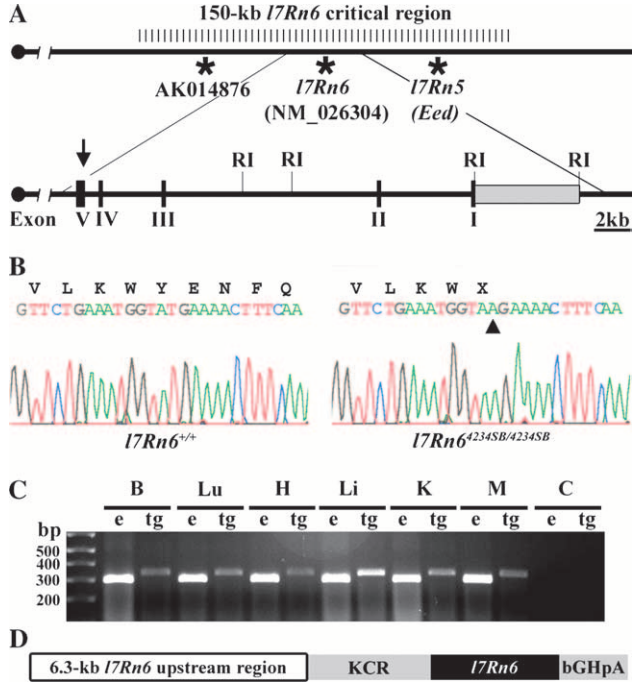

FIGURE 1.—Positional cloning of *l7Rn6*. (A) Gene order in the 150-kb *l7Rn6*-critical region on mouse chromosome 7. Complementation groups *l7Rn5* (*Eed*) and *l7Rn6* (NM_026304) are indicated. The third locus in the region AK014876 has not been represented in a complementation group. The enlarged map shows exon/intron organization of the *l7Rn6* gene. Arrow indicates the location of the ENU-induced T → A transversion. RI indicates *Eco*RI restriction sites. Gray box upstream of exon I indicates the 6.3-kb *Eco*RI fragment used as a promoter in the *l7Rn6* transgenic construct. The solid circle depicts the centromere. (B) Sequence analysis of *l7Rn6* in *l7Rn6*^{4234SB} homozygotes. The arrowhead denotes the T → A transversion at thymine 543 in the coding region of the *l7Rn6*^{4234SB} allele, which substitutes tyrosine 181 with a stop codon (Y181X). (C) Expression analysis of endogenous and transgenic *l7Rn6* mRNA. Semi-quantitative RT-PCR analysis of endogenous (e) and transgenic (tg) *l7Rn6* mRNA expression. Tissues included brain, B; lung, Lu; heart, H; liver, Li; kidney, K; and muscle, M. C, denotes water control. Note relatively low levels of transgenic *l7Rn6* expression. Results derive from analysis of the *A4tg* line. (D) Design of the transgenic construct used for *l7Rn6*^{4234SB} rescue experiments. A 6.3-kb *Eco*RI fragment encompassing the genomic region upstream of the first exon of *l7Rn6* (see Figure 1A) was used as promoter for the transgene. The KCR cassette with intronic sequences from the rabbit β-*globin* locus was inserted to augment transgene expression. A heterologous 3′-UTR containing the bovine growth hormone polyadenylation signal was cloned downstream of the full-length *l7Rn6* open reading frame.

Positional cloning of *l7Rn6*: Two complementation groups, *l7Rn5* and *l7Rn6*, were previously mapped to a 150-kb interval delineated by the *c*^{3H} and *c*^{AL} deletion breakpoints (RINCHIK and CARPENTER 1993; HOLDENER *et al.* 1995) (see also Figure 1A). The *l7Rn5* complementation group encompassed three alleles of the *Polycomb*-group gene *Eed* (SCHUMACHER *et al.* 1996). In contrast, *l7Rn6* was represented by a single allele, *l7Rn6*^{4234SB}. The

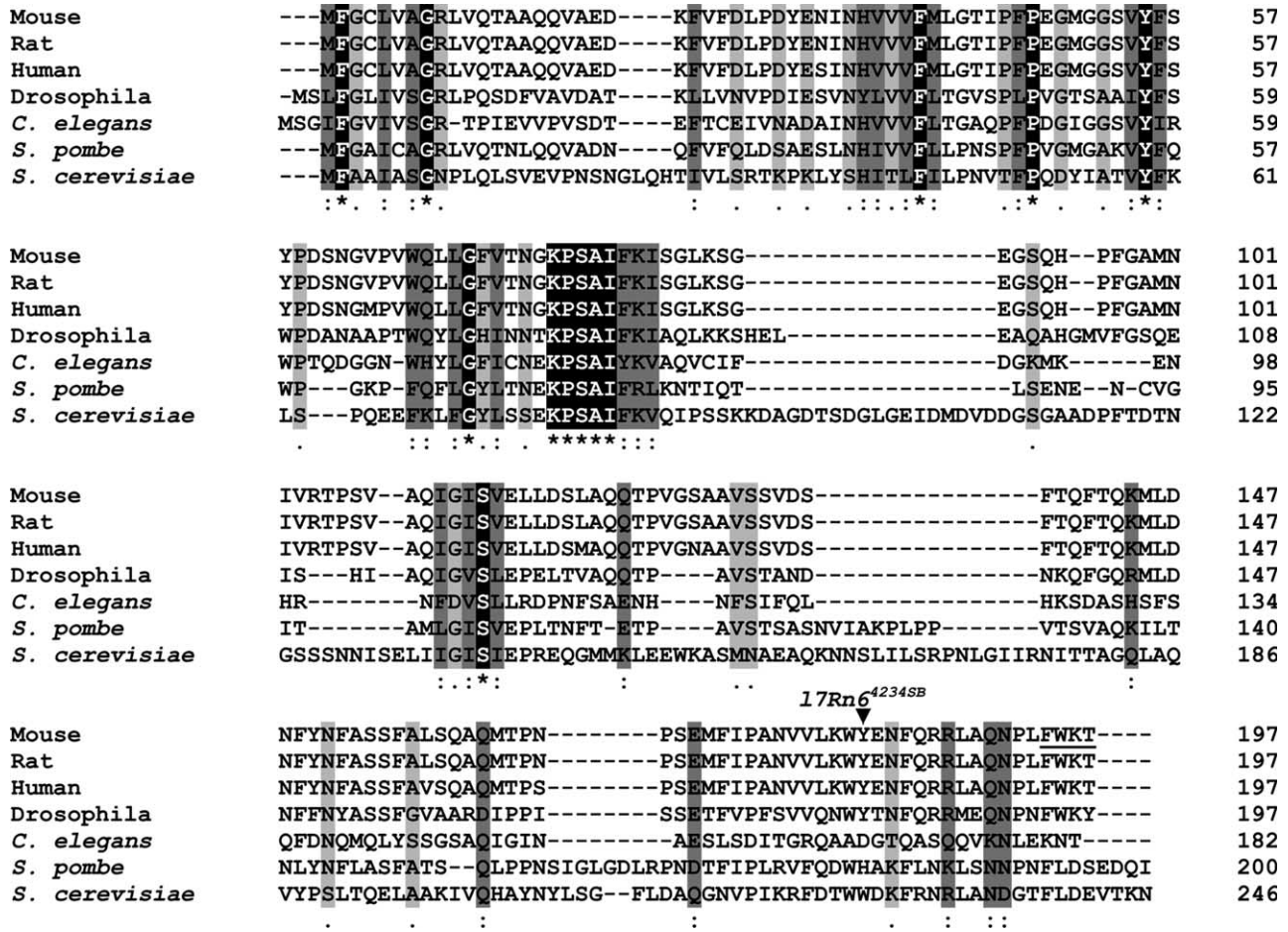

FIGURE 2.—Evolutionary conservation of the l7Rn6 protein. Protein sequence alignment of mouse l7Rn6 with rat, human, Drosophila, *Caenorhabditis elegans*, *Schizosaccharomyces pombe*, and *Saccharomyces cerevisiae* homologs. l7Rn6 Conserved residues (*) as well as conservative (:) and semiconservative (.) substitutions are indicated. Note that the region from W67 to I84 contains the distinctive motif KPSAI that, along with G71, is 100% conserved across species. The arrowhead denotes the ENU-induced mutation in *l7Rn6*^{4234SB}, which substitutes Y181 with a stop codon (Y181X), truncating the C-terminal 17 amino acids of the protein. The KKXX-like ER retention motif FWKT at the carboxy terminus is underlined.

strategy for cloning the *l7Rn6* locus involved identification of candidate transcription units in the vicinity of *Eed* from draft versions of the mouse and human genome sequence as well as EST databases. *l7Rn6* candidate genes were mapped relative to the critical 150-kb interval using YACs spanning the region (HOLDENER *et al.* 1995). Two candidate genes encoding hypothetical proteins were identified in the *l7Rn6* region: AK014876 and NM_026304 (Figure 1A). Following PCR amplification from *l7Rn6*$^{4234SB/4234SB}$ DNA, candidate genes were analyzed for sequence alterations absent from coisogenic *l7Rn5* alleles (RINCHIK and CARPENTER 1993). The coding region and untranslated regions of AK014876 displayed wild-type sequences (data not shown). In contrast, a T → A transversion was detected at thymine 543 of the NM_026304 coding region in *l7Rn6*^{4234SB} (Figure 1B). The T → A transversion encompassed the third nucleotide of codon 181 (TAT → TAA) and substituted a tyrosine residue with a stop codon (Y181X), truncating the carboxy-terminal 17 amino acids of the l7Rn6 protein (Figure 2). T → A transversions represent the most common type of ENU-induced mutations in the mouse germline, constituting approximately one-third of all mutations identified thus far (NOVEROSKE *et al.* 2000). Importantly, the three co-isogenic *l7Rn5* alleles exhibited the wild-type thymine 543 in the NM_026304 locus (Figure 1B and data not shown). Furthermore, the T → A transversion cosegregated invariably with the *l7Rn6*^{4234SB} mutant phenotype. No other sequence alterations were found and NM_026304 is herein referred to as the *l7Rn6* gene. On the basis of the University of California at Santa Cruz mouse genome assembly mm5 (build m33 NCBI) and consistent with our YAC mapping (data not shown), *l7Rn6* is located ~13 kb proximal to *Eed* and is composed of five exons, which span 23 kb in genomic DNA (Figure 1A). No gene sequences homologous to *l7Rn6* were identified in the mouse genome (data not shown). RT-PCR analysis indicated *l7Rn6* mRNA expression in all tissues analyzed, including brain, lung, heart, liver, kidney, and muscle (Figure 1C).

Partial transgenic rescue: The *l7Rn6* transgenic founders were generated on a pure FVB/NJ background and potential rescue of the *l7Rn6*^{4234SB} lung phenotype was assessed on a 75% FVB/NJ background. Surprisingly, homozygosity for the *l7Rn6*^{4234SB} mutation appeared embryonic lethal on this background since no *l7Rn6*$^{4234SB/4234SB}$ pups were recovered at birth. In contrast, 24 *l7Rn6*$^{4234SB/4234SB}$;*A4tg* pups were recovered among 90 pups at P0 from intercrosses between *l7Rn6*$^{4234SB/+}$;*A4tg* animals. Ten of these *l7Rn6*$^{4234SB/4234SB}$;*A4tg* pups were found dead at P0 and 7 died before P2. The remaining 7 animals died between P7 and P21. They appeared slightly runted at P0 but displayed grossly normal development over the next few days. Approximately 2 days before death, *l7Rn6*$^{4234SB/4234SB}$;*A4tg* animals became increasingly runted and lethargic. Thus, the *A4tg* transgenic line partially rescued the prenatal lethality of *l7Rn6*^{4234SB} homozygotes on a largely FVB/NJ background, confirming NM_026304 as the *l7Rn6* locus. The partial rescue is consistent with the relatively low expression level of both transgenic lines compared with endogenous *l7Rn6* (Figure 1C and data not shown), suggesting that the ~6.3-kb genomic promoter region lacked regulatory elements and/or was sensitive to repressive positional effects.

Protein sequence analysis of l7Rn6: *l7Rn6* encodes a 197-aa protein, which is highly conserved from yeast to mammals. Protein sequence identity ranges from 77 to 100% among vertebrates (Figure 2). Sequence alignment using ClustalW 1.74 and 1.82 revealed four highly conserved subsequences, mostly located in the amino-terminal half of the protein (Figure 2). The WQLLGFVTNGKPSAIFKI motif displays the highest evolutionary conservation, most prominently in the KPSAI subsequence, which exhibits 100% identity across all species, constituting a distinctive signature of this novel protein. PSORT II (Nakai and Kanehisa 1992) identified the FWKT sequence at the carboxy terminus of l7Rn6 as a KKXX-like, endoplasmic reticulum membrane retention signal. Other protein motifs, including nuclear localization signals, DNA-binding domains, or transmembrane domains, were not found (data not shown).

***l7Rn6*^{4234SB} homozygotes display emphysematous lungs at birth:** *l7Rn6*$^{4234SB/4234SB}$ lungs were remarkable for a discrete developmental delay during the canalicular stage (E16.5) (data not shown). At the beginning of the saccular stage (E17.5), *l7Rn6*$^{4234SB/4234SB}$ lung saccules appeared not fully dilated and resembled E16.5 wild-type lungs (Figure 3A and data not shown). However, as development proceeded, the delay became less evident (data not shown). At P0, the lung:body weight ratio revealed no statistically significant difference between *l7Rn6*$^{4234SB/4234SB}$ and *l7Rn6*$^{+/+}$ mice ($P > 0.05$) (Figure 3B). Furthermore, Periodic Acid Schiff (PAS) glycogen staining, a marker for perinatal lung maturity (Compernolle *et al.* 2002), detected no differences in lung glycogen content between *l7Rn6*$^{4234SB/4234SB}$ and wild-type littermates at P0 (data not shown).

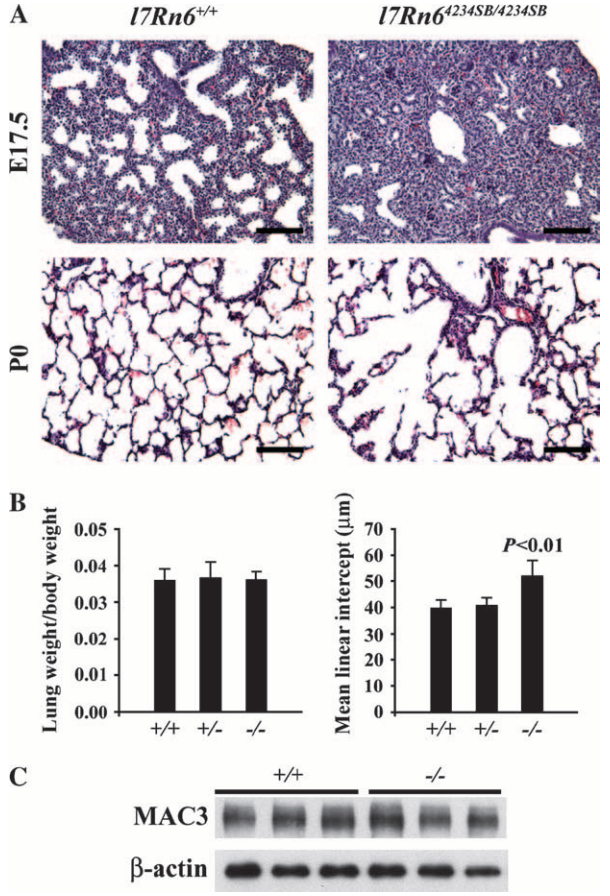

Figure 3.—Lung phenotype in *l7Rn6*^{4234SB} homozygotes. (A) H&E-stained sections from *l7Rn6*$^{+/+}$ and *l7Rn6*$^{4234SB/4234SB}$ lungs at E17.5 and P0. At E17.5, mutant lungs exhibited a discrete developmental delay compared with wild type. *l7Rn6*$^{4234SB/4234SB}$ lungs displayed a severe emphysematous phenotype at P0. Bar, 100 μm. (B) Lung morphometry. The lung:body weight ratio showed no statistically significant difference ($P > 0.05$) between *l7Rn6*$^{+/+}$, *l7Rn6*$^{4234/+}$, and *l7Rn6*$^{4234SB/4234SB}$ (represented as −/−), indicating that the *l7Rn6*^{4234SB} mutation did not affect lung growth. Analysis of the mean linear intercepts demonstrated a statistically significant difference ($P < 0.01$) in airway dilation between *l7Rn6*$^{+/+}$ and *l7Rn6*$^{4234SB/4234SB}$ mice. (C) No difference in MAC3 expression between wild-type and *l7Rn6*$^{4234SB/4234SB}$ lungs (represented as −/−).

Serial sections of lungs from *l7Rn6*^{4234SB} homozygotes demonstrated a significant emphysematous phenotype at birth (Figure 3A). The extent of distal airway dilation was quantified by analysis of the mean linear intercepts (Dunnill 1962) in *l7Rn6*$^{+/+}$ and *l7Rn6*$^{4234SB/4234SB}$ lungs. At P0, *l7Rn6*$^{4234SB/423SB}$ showed a statistically significant enlargement of the distal airways, with a mean linear intercept of 52.1 ± 6.2 μm compared with 39.8 ± 3.1 μm in *l7Rn6*$^{+/+}$ pups ($P < 0.01$) (Figure 3B). In the context of the emphysematous lung phenotype and frequent cyanosis in *l7Rn6*^{4234SB} homozygotes, we attribute the perinatal lethality to respiratory failure.

As demonstrated by Western blot analysis and immunohistochemistry for MAC3, a marker for alveolar

macrophages (Glasser *et al.* 2003), the distribution and number of macrophages appeared indistinguishable between *l7Rn6*$^{4234SB/4234SB}$ and wild-type littermates (Figure 3C and data not shown). In addition, mutant lungs were devoid of inflammatory infiltrates (Figure 3A).

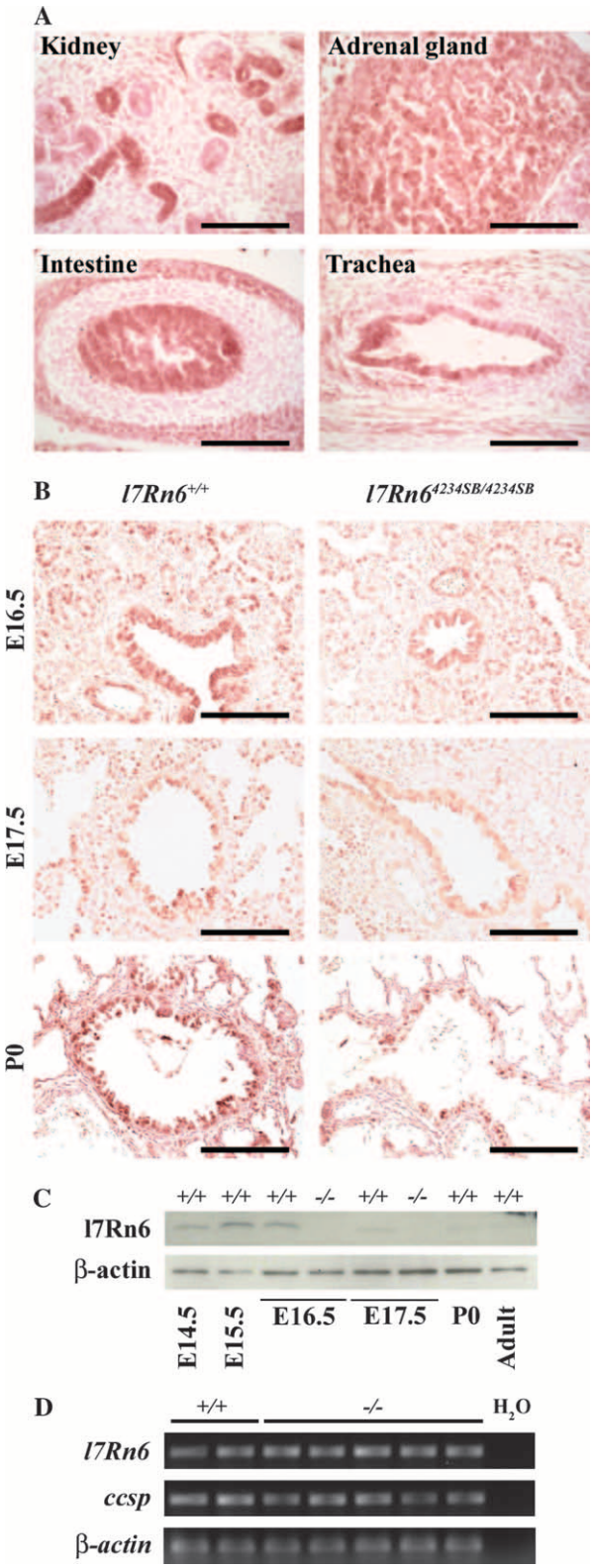

l7Rn6 expression and instability of the l7Rn6^{4234SB} protein: E15.5 embryos displayed cytoplasmic l7Rn6 protein expression in multiple tissues, including heart, kidney, adrenal gland, pituitary, submandibular glands, intestine, trachea, and lung (Figure 4A and data not shown). In the developing lung, l7Rn6 expression was detected in epithelial cells between E15.5 and E17.5 (Figure 4B and data not shown). At P0, l7Rn6 expression appeared restricted to the bronchiolar epithelium, including Clara cells (Figure 4B). There was no evidence for l7Rn6 expression in type II cells at P0 (Figure 4B). Western blot analysis confirmed significant l7Rn6 expression at E14.5-E16.5, which decreased toward late gestation (Figure 4C). At P0 as well as in adult lungs, l7Rn6 expression levels ranged barely above detection limits. Strikingly, immunohistochemistry and Western blot analysis, respectively, demonstrated a significant reduction and absence of l7Rn6 expression in *l7Rn6*^{4234SB} homozygous lungs (Figure 4, B and C). *l7Rn6* mRNA levels were indistinguishable between P0 wild-type and *l7Rn6*$^{4234SB/4234SB}$ lungs by semiquantitative RT-PCR (Figure 4D). Thus, the significant decrease in l7Rn6 protein levels in *l7Rn6*^{4234SB} homozygous lungs did not appear to result from nonsense-mediated mRNA decay, which frequently eliminates mRNAs with premature termination codons (Baker and Parker 2004). Additional evidence for *l7Rn6*^{4234SB} protein instability derived from transfection experiments in COS7 and HEK293 cells. Whereas tagged wild-type protein displayed abundant expression, a construct containing a cDNA truncated at the mutant stop codon consistently yielded significantly lower levels of *l7Rn6*^{4234SB} expression (data not shown). Therefore, the ENU-induced point mutation appeared to render the mutant protein unstable.

Normal cellular composition in *l7Rn6*^{4234SB} homozygous lungs: To characterize the various lung cell types between E15.5 and P0, we studied marker gene expression by immunohistochemistry on sections from wild-type and *l7Rn6*$^{4234SB/4234SB}$ lungs at P0. No differences in expression

Figure 4.—l7Rn6 protein expression. (A) Immunohistochemistry on sections from wild-type embryos revealed cytoplasmic l7Rn6 protein expression in kidney, adrenal gland, intestine, and trachea. Bar, 100 μm. (B) Lungs demonstrated l7Rn6 expression in epithelial cells at E16.5 and E17.5. At P0, expression was restricted to the bronchiolar epithelium. Note that l7Rn6 expression levels were significantly reduced in sections from *l7Rn6*$^{4234SB/4234SB}$ lungs at all stages analyzed. For accurate comparison of expression levels between genotypes, sections from mutant and wild-type lungs were mounted on the same slide. Bar, 100 μm. (C) Western blot analysis revealed l7Rn6 protein expression between E14.5 and P0 as well as in adult lung. Note that l7Rn6 was barely detectable at late gestation and in adult lungs. Strikingly, expression of the truncated l7Rn6^{4234SB} protein in *l7Rn6*$^{4234SB/4234SB}$ lungs (represented as −/−) was undetectable by Western blot analysis. (D) Semi-quantitative RT-PCR analysis of *l7Rn6* and *ccsp* mRNA levels revealed comparable transcript levels between wild-type and *l7Rn6*$^{4234SB/4234SB}$ P0 lungs (represented as −/−).

of SP-C and CGRP were detected between wild-type and *l7Rn6*^{4234SB} homozygotes, suggesting that type II cells and neuroendocrine cells were present in normal numbers and distribution at P0 (Figure 5). Immunohistochemistry for CC26, a selenium-independent glutathione peroxidase expressed specifically in Clara cells (Power and Nicholas 1999), detected no difference in expression between wild-type and mutant lungs (Figure 5). Furthermore, there was no difference in the number of Clara cells expressing SP-A (Figure 5). On the basis of expression of MAC-3 and α-smooth muscle actin, the macrophage and alveolar myofibroblast cell population, respectively, also appeared indistinguishable between *l7Rn6*$^{4234SB/4234SB}$ and wild-type littermates (Figure 3C and data not shown). Thus, these results suggest that the *l7Rn6*^{4234SB} mutation did not affect the cellular composition of the lung.

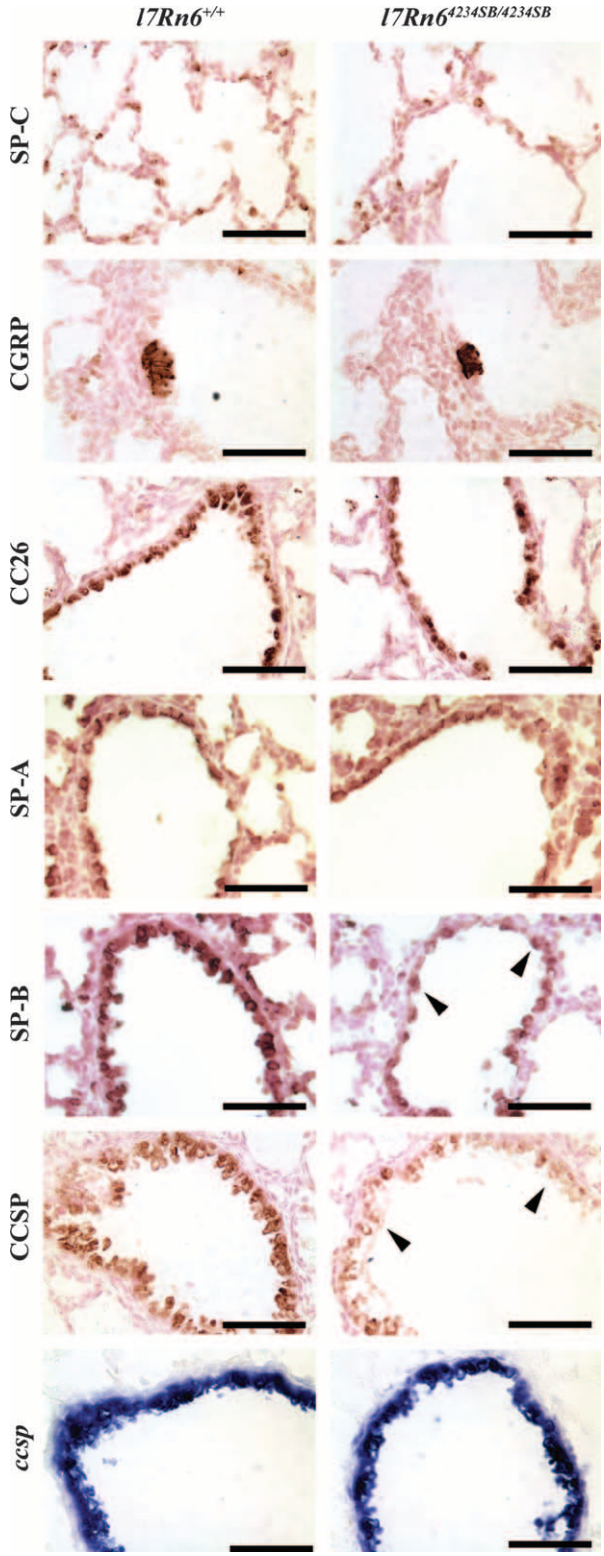

A defect in Clara cell function in *l7Rn6*^{4234SB} homozygous lungs: Strikingly, expression levels of cytoplasmic CCSP and SP-B were significantly decreased in Clara cells from *l7Rn6*$^{4234SB/4234SB}$ lungs compared with wild-type littermates (Figure 5). The decrease in CCSP and SP-B expression was consistently detected in sections from *l7Rn6*$^{4234SB/4234SB}$ lungs compared with *l7Rn6*$^{+/+}$ sections mounted side by side on the same slide. To ascertain a potential mechanism of decreased cytoplasmic CCSP expression, we performed mRNA *in situ* hybridization with a *ccsp* antisense probe. As demonstrated in Figure 5, *ccsp* mRNA levels and distribution in wild-type and mutant lungs were indistinguishable at P0. In addition, semiquantitative RT-PCR revealed no differences in *ccsp* mRNA levels between wild-type and mutant lungs (Figure 4D). These data implicate an unknown post-transcriptional, presumably post-translational mechanism in decreased expression of cytoplasmic CCSP.

Taken together, the *l7Rn6*^{4234SB} mutation disrupted Clara cell function as evidenced by decreased levels of CCSP and SP-B expression. However, a general defect in protein expression in Clara cells appeared less likely since CC26 and SP-A expression levels were indistinguishable between wild-type and *l7Rn6*^{4234SB} mutant lungs (Figure 5).

Subcellular localization of l7Rn6: Indirect immunofluorescence in A549 lung carcinoma cells detected largely punctate l7Rn6 signal throughout the cytoplasm. l7Rn6 did not colocalize with GS28, which marks the *cis*-Golgi complex (Subramaniam *et al.* 1996), in A549, HEK293, and COS7 cells (Figure 6 and data not shown). However, l7Rn6 exhibited significant colocalization in the perinuclear region with Calnexin, a marker for the endoplasmic reticulum (Wada *et al.* 1991) (Figure 6).

Figure 5.—Marker gene expression analysis in *l7Rn6*^{4234SB} homozygous lungs. Immunohistochemistry on P0 lung sections showed no significant differences in SP-C, CGRP, CC26, and SP-A expression between *l7Rn6*$^{+/+}$ and *l7Rn6*$^{4234SB/4234SB}$ lungs. In contrast, SP-B and CCSP expression in Clara cells was consistently reduced in *l7Rn6*$^{4234SB/4234SB}$ compared with wild-type lungs mounted side by side on the same slide. mRNA *in situ* hybridization using an antisense *ccsp* cRNA probe revealed no differences between *l7Rn6*$^{+/+}$ and *l7Rn6*$^{4234SB/4234SB}$ lungs. As a control, a *ccsp* sense probe yielded no signal (data not shown). Bars, 50 μm.

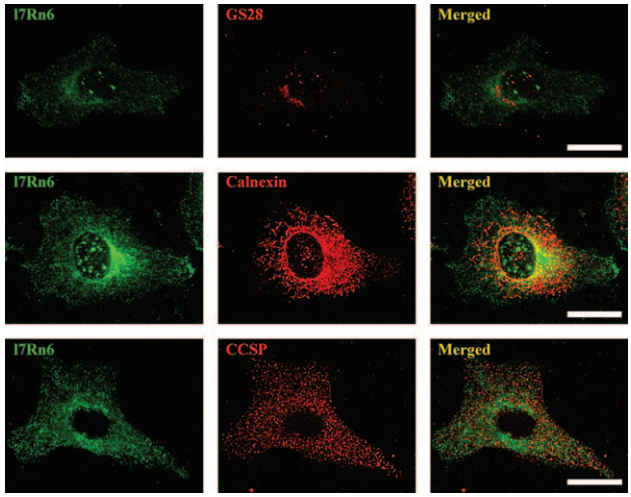

Figure 6.—Subcellular localization of l7Rn6. Indirect immunofluorescence detected mostly punctate staining of l7Rn6 throughout the cytoplasm in A549 lung carcinoma cells. l7Rn6 partially colocalized with Calnexin, a marker for the ER, but not with GS28, a marker for the *cis*-Golgi complex. Similar to l7Rn6, CCSP showed punctate staining throughout the cytoplasm but colocalization of the two proteins could not be detected. Bar, 20 μm.

Interestingly, l7Rn6 and CCSP did not colocalize in A549 cells (Figure 6), despite concomitant reduction of their protein levels in *l7Rn6*$^{4234SB/4234SB}$ lungs (Figure 4B and C).

Clara cell abnormalities in *l7Rn6*^{4234SB} homozygotes: Electron microscopy revealed an overall normal cellular organization and glycogen content of Clara cells in *l7Rn6*^{4234SB} homozygotes compared with wild type at P0 (Figure 7A). However, mutant Clara cells were remarkable for defects in the secretory apparatus, including enlargement and disorganization of the Golgi complex (Figure 7, A and B). Furthermore, abnormal vesicular structures of varying size and number were frequently detected in the cytoplasm of *l7Rn6*^{4234SB} homozygous Clara cells (Figure 7, A and C). These structures contained circular membranes and glycogen-like particles and were commonly found in close apposition to the Golgi complex (Figure 7, A and C). Mutant Clara cells presented no other defects in the cytoplasm or the nucleus. Other lung epithelial cells, such as type II cells, were devoid of ultrastructural abnormalities, including the secretory apparatus (data not shown).

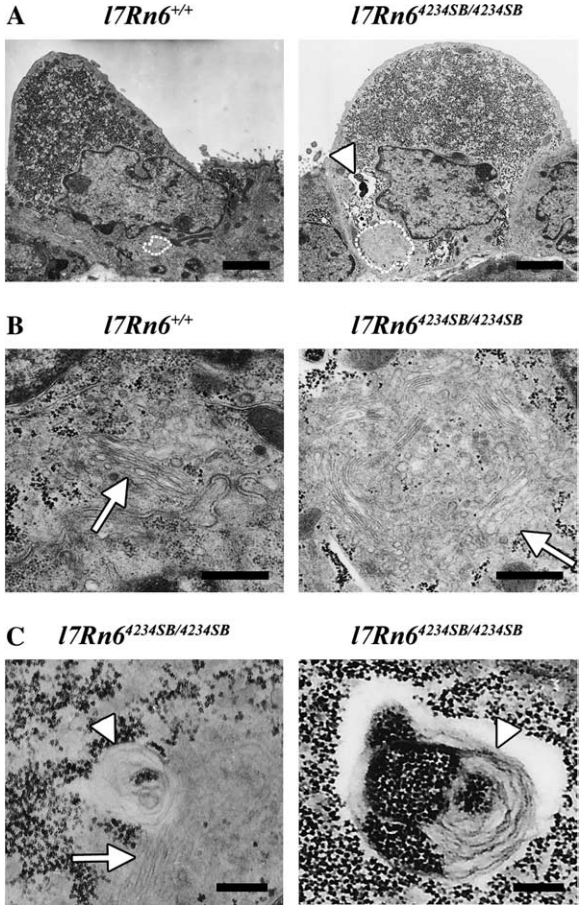

Figure 7.—Ultrastructural analysis of Clara cells from *l7Rn6*^{4234SB} homozygous. (A) Transmission electron microscopy demonstrated enlargement of the Golgi complex (dotted lines) and aberrant vesicular structures in the cytoplasm of *l7Rn6*$^{4234SB/4234SB}$ Clara cells (arrowhead). Bar, 2 μm. (B) High magnification of areas delineated by dotted lines in A. Compared with wild type, the Golgi apparatus in Clara cells from *l7Rn6*$^{4234SB/4234SB}$ lungs revealed significant abnormalities, including a marked enlargement and disorganization. Bar, 500 nm. (C) Left: High magnification revealed close apposition of an aberrant vesicular structure (arrowhead) to the Golgi apparatus (arrow) in *l7Rn6*$^{4234SB/4234SB}$ Clara cells. Left and right: Aberrant vesicular structures were filled with circular membranous material as well as glycogen-like particles in *l7Rn6*$^{4234SB/4234SB}$ Clara cells. Bar, 200 nm.

DISCUSSION

In recent years, significant progress has been made in dissecting the genetic control of mammalian lung development. Many transcription factors, peptide growth factors and their receptors, as well as extracellular matrix components have been identified as important regulators of lung morphogenesis in reverse genetics approaches (Warburton *et al.* 2000; Groenman *et al.* 2004; Kumar and Ryan 2004). Chemical mutagenesis using the potent germline mutagen ENU represents a powerful means to complement these gene-driven approaches by phenotype-based screens in mice (De Angelis *et al.* 2000; Nolan *et al.* 2000; Kile *et al.* 2003). This report describes the positional cloning of the perinatal lethal, ENU-induced *l7Rn6*^{4234SB} allele and identifies a pivotal role for the previously hypothetical gene NM_026304 in Clara cell function during mouse lung development. The ENU-induced nonsense mutation truncated the carboxy-terminal 17 aa, rendering the l7Rn6^{4234SB} protein unstable. However, detection of residual amounts of the mutant protein by immunohistochemistry

suggested that *l7Rn6*^{4234SB} constitutes a strong hypomorphic rather than a null allele. Partial transgenic rescue and absence of nucleotide alterations in all other known or hypothetical genes in the 150-kb critical region revealed NM_026304 as the causative gene for the *l7Rn6*^{4234SB} phenotype.

l7Rn6 protein expression was detected in several epithelial and secretory tissues during embryonic development, including kidney, adrenal gland, intestine, trachea, and lung. Evidence for abnormal Clara cell function derived from a significant decrease in intracellular CCSP and SP-B levels. Since expression levels of CC26 and SP-A were indistinguishable between wild-type and *l7Rn6*^{4234SB} homozygotes, a general decrease in proteins secreted by Clara cells appeared less likely. Interestingly, previous yeast two-hybrid screening identified physical interaction of YOL032W and Sec17, the Saccharomyces homolog of l7Rn6 and α-SNAP, respectively (Uetz *et al.* 2000; Hazbun *et al.* 2003). α-SNAP governs a crucial step in vesicle fusion (Bonifacino and Glick 2004) and has recently been implicated in surfactant secretion in type II pneumocytes (Abonyo *et al.* 2003). However, we could not detect colocalization of l7Rn6 and α-SNAP in COS7, HEK293, and A549 cells (data not shown).

KKXX motif-containing proteins typically reside in the endoplasmic reticulum (ER) and participate in the retrograde transport of COPI vesicles from the Golgi complex to the ER (Lee *et al.* 2003; Stornaiuolo *et al.* 2003; Bonifacino and Glick 2004). A carboxy-terminal KKXX-like motif in the l7Rn6 protein, which is ablated by the *l7Rn6*^{4234SB} nonsense mutation, partial colocalization with Calnexin, and decreased levels of secreted proteins such as CCSP and SP-B, portend a role for l7Rn6 in the secretory apparatus. Indeed, aberrant vesicular structures, filled with membranous and glycogen-like material, were frequently detected in close apposition to an enlarged and disorganized Golgi complex in Clara cells from *l7Rn6*^{4234SB} homozygotes. Thus, this study established l7Rn6 as a novel protein with a potential function in vesicular trafficking between the ER and Golgi complex.

Phenotypic and marker gene expression analysis revealed that homozygosity for the *l7Rn6*^{4234SB} allele did not appear to affect early lung patterning, growth, or cellular differentiation. Rather, *l7Rn6*$^{4234SB/4234SB}$ lungs demonstrated an emphysematous enlargement of the terminal respiratory sacs. Emphysematous phenotypes have been described in multiple mouse models and various disease mechanisms have been identified. For example, mice doubly homozygous for mutant alleles of *Fgfr3* and *Fgfr4* showed an emphysematous phenotype and lack of alveologenesis due to failure in secondary septation and increased elastin deposition (Weinstein *et al.* 1998). *Pdgfa*-deficient mice exhibited atelectasis and emphysema secondary due to a failure in alveolar septation, which, in turn, resulted from a loss of alveolar myofibroblasts and parenchymal elastin deposition (Boström *et al.* 1996, 2002). Likewise, loss of function of the tissue inhibitor of metalloproteinases-3 (*Timp3*) led to an emphysematous phenotype by the second week of life, enhanced degradation of collagen in the peribronchiolar space, and decreased bronchiolar branching (Leco *et al.* 2001; Gill *et al.* 2003). Whereas most of these mouse mutants developed emphysematous phenotypes with age, loss of function of Fibrillin-1 caused emphysema formation as early as P1 (Neptune *et al.* 2003). Given similar early-onset emphysema in *l7Rn6*^{4234SB} homozygotes, we considered potential defects in extracellular matrix components as a contributing factor in disease pathogenesis. However, preliminary analysis revealed no differences in parenchymal elastin content and tissue distribution of myofibroblasts between wild-type and *l7Rn6*^{4234SB} homozygous lungs (data not shown). Furthermore, the perinatal death of *l7Rn6*^{4234SB} homozygotes preceeds alveolar septation, which occurs between P5 and P30 in mice (Ten Have-Opbroek 1991; Warburton *et al.* 2000). This renders a septation defect as a contributing factor in the pathogenesis of the emphysematous lung phenotype less likely.

Several mouse mutants exhibited pulmonary emphysema in the presence of inflammation. For example, overexpression of *Pdgfb* caused emphysematous lesions, inflammation, as well as lung fibrosis (Hoyle *et al.* 1999). Loss of integrin αvβ6 (*Itgb6*)-mediated TGF-β activation caused age-related emphysema, inflammation, and upregulation of the macrophage metalloelastase Mmp12 (Morris *et al.* 2003). Mice deficient for SP-C developed progressive emphysema, type-II cell hyperplasia, pneumonitis, and upregulation of several metalloproteinases, including Mmp12 (Glasser *et al.* 2003). However, analysis of *Timp3*-mutant mice and double homozygotes for null alleles of *Itgb6* and *Mmp12* demonstrated that inflammation is not required for the development of emphysema (Leco *et al.* 2001; Gill *et al.* 2003; Morris *et al.* 2003). Indeed, the emphysematous enlargement of the respiratory sacs in *l7Rn6*$^{4234SB/4234SB}$ lungs was devoid of inflammatory infiltrates and changes in the tissue distribution or number of alveolar macrophages.

This raises the question as to whether the emphysematous enlargement of the terminal respiratory sacs and perinatal death of *l7Rn6*^{4234SB} homozygotes could result from a secretory defect in Clara cells. In support of this notion, deletion of Foxa2 resulted in emphysematous enlargement of the lungs in the context of decreased expression levels of several secreted proteins, including CCSP, SP-A, SP-C, and SP-B (Wan *et al.* 2004a,b). SP-B deficiency in mice caused respiratory failure and death shortly after birth (Clark *et al.* 1995). Interestingly, these mutants also demonstrated reduced levels of SP-C, an abnormal Golgi apparatus and large, atypical intracellular membranous inclusions in cells of the respiratory epithelium. Likewise, Clara cells in *ccsp*-deficient mice revealed an enlarged Golgi complex and concentric whorls of endoplasmic reticulum (Stripp *et al.* 2002), although animal viability was unaffected in

two different mutant lines (Stripp *et al.* 1996; Zhang *et al.* 1997). Thus, *l7Rn6^{4234SB}* homozygotes share certain phenotypic features with these mutants and decreased levels of CCSP and SP-B expression might indeed play a significant role in the development of the perinatal emphysematous enlargement and lung failure.

We are grateful to Terry Magnuson and Gene Rinchik for providing the *l7Rn6^{4234SB}* mutant strain. We thank James Barrish (Department of Pathology, Texas Children's Hospital) for electron microscopy, Richard Atkinson for help with confocal microscopy, Gerard Karsenty for generous microscope access, and Miriam Mendoza for technical assistance. Francesco DeMayo as well as members of our laboratory are acknowledged for helpful discussions and critical reading of the manuscript. This work was supported by a research grant from the National Institutes of Health to A.S.

LITERATURE CITED

Abonyo, B. O., P. Wang, T. A. Narasaraju, W. H. Rowan, III, D. H. Mcmillan *et al.*, 2003 Characterization of alpha-soluble N-ethylmaleimide-sensitive fusion attachment protein in alveolar type II cells: implications in lung surfactant secretion. Am. J. Respir. Cell Mol. Biol. **29:** 273–282.

Baker, K. E., and R. Parker, 2004 Nonsense-mediated mRNA decay: terminating erroneous gene expression. Curr. Opin. Cell Biol. **16:** 293–299.

Blundell, R. A., and D. J. Harrison, 2005 Integrin characterization in pulmonary bronchioles. Exp. Mol. Pathol. **79:** 74–78.

Bonifacino, J. S., and B. S. Glick, 2004 The mechanisms of vesicle budding and fusion. Cell **116:** 153–166.

Boström, H., K. Willetts, M. Pekny, P. Leveen, P. Lindahl *et al.*, 1996 PDGF-A signaling is a critical event in lung alveolar myofibroblast development and alveogenesis. Cell **85:** 863–873.

Boström, H., A. Gritli-Linde and C. Betsholtz, 2002 PDGF-A/PDGF alpha-receptor signaling is required for lung growth and the formation of alveoli but not for early lung branching morphogenesis. Dev. Dyn. **223:** 155–162.

Broeckaert, F., A. Clippe, B. Knoops, C. Hermans and A. Bernard, 2000 Clara cell secretory protein (CC16): features as a peripheral lung biomarker. Ann. NY Acad. Sci. **923:** 68–77.

Chen, L. C., Z. J. Zhang, A. C. Myers and S. K. Huang, 2001 Cutting edge: Altered pulmonary eosinophilic inflammation in mice deficient for Clara cell secretory 10-kDa protein. J. Immunol. **167:** 3025–3028.

Clark, J. C., S. E. Wert, C. J. Bachurski, M. T. Stahlman, B. R. Stripp *et al.*, 1995 Targeted disruption of the surfactant protein B gene disrupts surfactant homeostasis, causing respiratory failure in newborn mice. Proc. Natl. Acad. Sci. USA **92:** 7794–7798.

Cole, F. S., A. Hamvas and L. M. Nogee, 2001 Genetic disorders of neonatal respiratory function. Pediatr. Res. **50:** 157–162.

Compernolle, V., K. Brusselmans, T. Acker, P. Hoet, M. Tjwa *et al.*, 2002 Loss of HIF-2alpha and inhibition of VEGF impair fetal lung maturation, whereas treatment with VEGF prevents fatal respiratory distress in premature mice. Nat. Med. **8:** 702–710.

De Angelis, M. H., H. Flaswinkel, H. Fuchs, B. Rathkolb, D. Soewarto *et al.*, 2000 Genome-wide, large-scale production of mutant mice by ENU mutagenesis. Nat. Genet. **25:** 444–447.

Dunnill, M. S., 1962 Quantitative methods in the study of the pulmonary pathology. Thorax **17:** 320–328.

Evans, M. J., L. V. Johnson, R. J. Stephens and G. Freeman, 1976 Renewal of the terminal bronchiolar epithelium in the rat following exposure to NO2 or O3. Lab. Invest. **35:** 246–257.

Evans, M. J., L. J. Cabral-Anderson and G. Freeman, 1978 Role of the Clara cell in renewal of the bronchiolar epithelium. Lab. Invest. **38:** 648–653.

Gill, S. E., M. C. Pape, R. Khokha, A. J. Watson and K. J. Leco, 2003 A null mutation for *tissue inhibitor of metalloproteinases-3* (*Timp-3*) impairs murine bronchiole branching morphogenesis. Dev. Biol. **261:** 313–323.

Glasser, S. W., E. A. Detmer, M. Ikegami, C. L. Na, M. T. Stahlman *et al.*, 2003 Pneumonitis and emphysema in *sp-C* gene targeted mice. J. Biol. Chem. **278:** 14291–14298.

Groenman, F., S. Unger and M. Post, 2004 The molecular basis for abnormal human lung development. Biol. Neonate **87:** 164–177.

Hazbun, T. R., L. Malmstrom, S. Anderson, B. J. Graczyk, B. Fox *et al.*, 2003 Assigning function to yeast proteins by integration of technologies. Mol. Cell **12:** 1353–1365.

Holdener, B. C., J. W. Thomas, A. Schumacher, M. D. Potter, E. M. Rinchik *et al.*, 1995 Physical localization of *Eed* - a region of mouse chromosome-7 required for gastrulation. Genomics **27:** 447–456.

Hoyle, G. W., J. Li, J. B. Finkelstein, T. Eisenberg, J. Y. Liu *et al.*, 1999 Emphysematous lesions, inflammation, and fibrosis in the lungs of transgenic mice overexpressing platelet-derived growth factor. Am. J. Pathol. **154:** 1763–1775.

Johnston, C. J., G. W. Mango, J. N. Finkelstein and B. R. Stripp, 1997 Altered pulmonary response to hyperoxia in Clara cell secretory protein deficient mice. Am. J. Respir. Cell Mol. Biol. **17:** 147–155.

Kalina, M., R. J. Mason and J. M. Shannon, 1992 Surfactant protein C is expressed in alveolar type II cells but not in Clara cells of rat lung. Am. J. Respir. Cell Mol. Biol. **6:** 594–600.

Kile, B. T., K. E. Hentges, A. T. Clark, H. Nakamura, A. P. Salinger *et al.*, 2003 Functional genetic analysis of mouse chromosome 11. Nature **425:** 81–86.

Kumar, V. H., and R. M. Ryan, 2004 Growth factors in the fetal and neonatal lung. Front. Biosci. **9:** 464–480.

Leco, K. J., P. Waterhouse, O. H. Sanchez, K. L. M. Gowing, A. R. Poole *et al.*, 2001 Spontaneous air space enlargement in the lungs of mice lacking tissue inhibitor of metalloproteinases-3 (TIMP-3). J. Clin. Invest. **108:** 817–829.

Lee, M. C., E. A. Miller, J. Golderg, L. Orci and R. Schekman, 2003 Bi-directional protein transport between the ER and Golgi. Annu. Rev. Cell Dev. Biol. **20:** 87–123.

Ma, Z. Q., S. S. Chua, F. J. Demayo and S. Y. Tsai, 1999 Induction of mammary gland hyperplasia in transgenic mice over-expressing human Cdc25B. Oncogene **18:** 4564–4576.

Mango, G. W., C. J. Johnston, S. D. Reynolds, J. N. Finkelstein, C. G. Plopper *et al.*, 1998 Clara cell secretory protein deficiency increases oxidant stress response in conducting airways. Am. J. Physiol. **275:** L348–L356.

Mok, H., J. Jelinek, S. Pai, B. M. Cattanach, J. T. Prchal *et al.*, 2004a Disruption of ferroportin 1 regulation causes dynamic alterations in iron homeostasis and erythropoiesis in polycythaemia mice. Development **131:** 1859–1868.

Mok, H., M. Mendoza, J. T. Prchai, P. Balogh and A. Schumacher, 2004b Dysregulation of ferroportin 1 interferes with spleen organogenesis in polycythaemia mice. Development **131:** 4871–4881.

Morris, D. G., X. Z. Huang, N. Kaminski, Y. N. Wang, S. D. Shapiro *et al.*, 2003 Loss of integrin alpha v beta 6-mediated TGF-beta activation causes Mmp12-dependent emphysema. Nature **422:** 169–173.

Nakai, K., and M. Kanehisa, 1992 A knowledge base for predicting protein localization sites in eukaryotic cells. Genomics **14:** 897–911.

Neptune, E. R., P. A. Frischmeyer, D. E. Arking, L. Myers, T. E. Bunton *et al.*, 2003 Dysregulation of TGF-beta activation contributes to pathogenesis in Marfan syndrome. Nat. Genet. **33:** 407–411.

Neubüser, A., H. Koseki and R. Balling, 1995 Characterization and developmental expression of *Pax9*, a paired-box-containing gene related to *Pax1*. Dev. Biol. **170:** 701–716.

Nogee, L. M., G. Garnier, H. C. Dietz, L. Singer, A. M. Murphy *et al.*, 1994 A mutation in the surfactant protein B gene responsible for fatal neonatal respiratory disease in multiple kindreds. J. Clin. Invest. **93:** 1860–1863.

Nolan, P. M., J. Peters, M. Strivens, D. Rogers, J. Hagan *et al.*, 2000 A systematic, genome-wide, phenotype-driven mutagenesis programme for gene function studies in the mouse. Nat. Genet. **25:** 440–443.

Noveroske, J. K., J. S. Weber and M. J. Justice, 2000 The mutagenic action of N-ethyl-N-nitrosourea in the mouse. Mamm. Genome **11:** 478–483.

Phelps, D. S., and J. Floros, 1991 Localization of pulmonary surfactant proteins using immunohistochemistry and tissue in situ hybridization. Exp. Lung Res. **17:** 985–995.

Power, J. H., and T. E. Nicholas, 1999 Immunohistochemical localization and characterization of a rat Clara cell 26-kDa protein (CC26) with similarities to glutathione peroxidase and phospholipase A2. Exp. Lung Res. **25:** 379–392.

Ramsay, P. L., F. J. Demayo, S. E. Hegemier, M. E. Wearden, C. V. Smith *et al.*, 2001 Clara cell secretory protein oxidation and expression in premature infants who develop bronchopulmonary dysplasia. Am. J. Respir. Crit. Care Med. **164:** 155–161.

Ray, M. K., G. Wang, J. Barrish, M. J. Finegold and F. J. Demayo, 1996 Immunohistochemical localization of mouse Clara cell 10-KD protein using antibodies raised against the recombinant protein. J. Histochem. Cytochem. **44:** 919–927.

Rinchik, E. M., and D. A. Carpenter, 1993 N-Ethyl-N-Nitrosourea-induced prenatally lethal mutations define at least 2 complementation groups within the embryonic ectoderm development (*Eed*) locus in mouse chromosome-7. Mamm. Genome **4:** 349–353.

Rinchik, E. M., and D. A. Carpenter, 1999 *N*-ethyl-*N*-nitrosourea mutagenesis of a 6- to 11-cM subregion of the *Fah-Hbb* interval of mouse chromosome 7: completed testing of 4557 gametes and deletion mapping and complementation analysis of 31 mutations. Genetics **152:** 373–383.

Rinchik, E. M., D. A. Carpenter and P. B. Selby, 1990 A strategy for fine-structure functional analysis of a 6- to 11-centimorgan region of mouse chromosome-7 by high-efficiency mutagenesis. Proc. Natl. Acad. Sci. USA **87:** 896–900.

Schumacher, A., C. Faust and T. Magnuson, 1996 Positional cloning of a global regulator of anterior-posterior patterning in mice. Nature **383:** 250–253.

Shulenin, S., L. M. Nogee, T. Annilo, S. E. Wert, J. A. Whitsett *et al.*, 2004 ABCA3 gene mutations in newborns with fatal surfactant deficiency. N. Engl. J. Med. **350:** 1296–1303.

Singh, G., and S. L. Katyal, 2000 Clara cell proteins. Ann. NY. Acad. Sci. **923:** 43–58.

Stornaiuolo, M., L. V. Lotti, N. Borgese, M. R. Torrisi, G. Mottola *et al.*, 2003 KDEL and KKXX retrieval signals appended to the same reporter protein determine different trafficking between endoplasmic reticulum, intermediate compartment, and Golgi complex. Mol. Biol. Cell **14:** 889–902.

Stripp, B. R., J. Lund, G. W. Mango, K. C. Doyen, C. Johnston *et al.*, 1996 Clara cell secretory protein: a determinant of PCB bioaccumulation in mammals. Am. J. Physiol. **271:** L656–L664.

Stripp, B. R., S. D. Reynolds, I. M. Boe, J. Lund, J. H. T. Power *et al.*, 2002 Clara cell secretory protein deficiency alters Clara cell secretory apparatus and the protein composition of airway lining fluid. Am. J. Respir. Cell Mol. Biol. **27:** 170–178.

Subramaniam, V. N., F. Peter, R. Philp, S. H. Wong and W. Hong, 1996 GS28, a 28-kilodalton Golgi SNARE that participates in ER-Golgi transport. Science **272:** 1161–1163.

Ten Have-Opbroek, A. A., 1991 Lung development in the mouse embryo. Exp. Lung Res. **17:** 111–130.

Tepera, S. B., P. D. Mccrea and J. M. Rosen, 2003 A beta-catenin survival signal is required for normal lobular development in the mammary gland. J. Cell Sci. **116:** 1137–1149.

Uetz, P., L. Giot, G. Cagney, T. A. Mansfield, R. S. Judson *et al.*, 2000 A comprehensive analysis of protein-protein interactions in *Saccharomyces cerevisiae*. Nature **403:** 623–627.

Wada, I., D. Rindress, P. H. Cameron, W. J. Ou, J. J. Doherty *et al.*, 1991 SSR alpha and associated calnexin are major calcium binding proteins of the endoplasmic reticulum membrane. J. Biol. Chem. **266:** 19599–19610.

Wan, H., K. H. Kaestner, S. L. Ang, M. Ikegami, F. D. Finkelman *et al.*, 2004a Foxa2 regulates alveolarization and goblet cell hyperplasia. Development **131:** 953–964.

Wan, H., Y. Xu, M. Ikegami, M. T. Stahlman, K. H. Kaestner *et al.*, 2004b *Foxa2* is required for transition to air breathing at birth. Proc. Nat. Acad. Sci. USA **101:** 14449–14454.

Warburton, D., M. Schwarz, D. Tefft, G. Flores-Delgado, K. D. Anderson *et al.*, 2000 The molecular basis of lung morphogenesis. Mech. Dev. **92:** 55–81.

Watson, T. M., S. D. Reynolds, G. W. Mango, I. M. Boe, J. Lund *et al.*, 2001 Altered lung gene expression in CCSP-null mice suggests immunoregulatory roles for Clara cells. Am. J. Physiol. Lung Cell. Mol. Physiol. **281:** L1523–L1530.

Weinstein, M., X. L. Xu, K. Ohyama and C. X. Deng, 1998 FGFR-3 and FGFR-4 function cooperatively to direct alveogenesis in the murine lung. Development **125:** 3615–3623.

Wilkinson, D. G., and M. A. Nieto, 1993 Detection of messenger RNA by in situ hybridization to tissue sections and whole mounts. Methods Enzymol. **225:** 361–373.

Zhang, Z. J., G. C. Kundu, C. J. Yuan, J. M. Ward, E. J. Lee *et al.*, 1997 Severe fibronectin-deposit renal glomerular disease in mice lacking uteroglobin. Science **276:** 1408–1412.

Communicating editor: K. V. Anderson